

# Mitigating reentry radio blackout by using a traveling magnetic field

Cite as: AIP Advances 7, 105314 (2017); <https://doi.org/10.1063/1.4999039>

Submitted: 04 August 2017 • Accepted: 10 October 2017 • Published Online: 19 October 2017

 Hui Zhou, Xiaoping Li, Kai Xie, et al.

## COLLECTIONS

 This paper was selected as an Editor's Pick



View Online



Export Citation



CrossMark

## ARTICLES YOU MAY BE INTERESTED IN

[An electromagnetic method for removing the communication blackout with a space vehicle upon re-entry into the atmosphere](#)

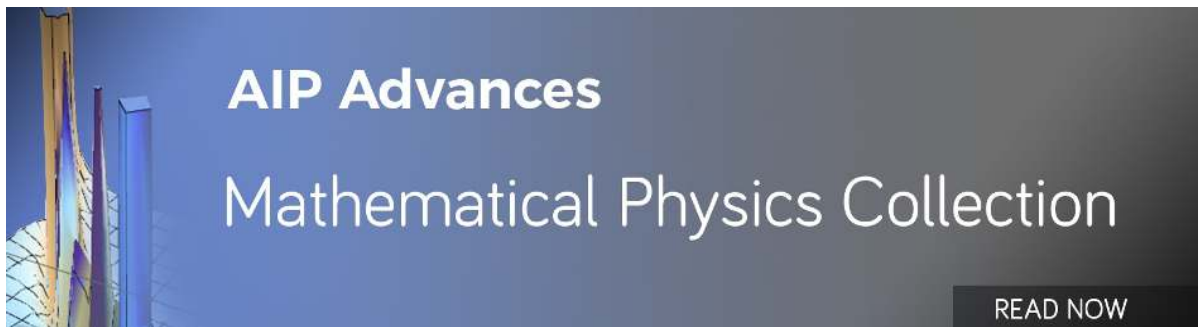
Journal of Applied Physics **121**, 093301 (2017); <https://doi.org/10.1063/1.4976213>

[A matching approach to communicate through the plasma sheath surrounding a hypersonic vehicle](#)

Journal of Applied Physics **117**, 233301 (2015); <https://doi.org/10.1063/1.4921751>

[Re-entry communication through a plasma sheath using standing wave detection and adaptive data rate control](#)

Journal of Applied Physics **119**, 023301 (2016); <https://doi.org/10.1063/1.4939700>



AIP Advances  
Mathematical Physics Collection

READ NOW

## Mitigating reentry radio blackout by using a traveling magnetic field

Hui Zhou,<sup>1,a</sup> Xiaoping Li,<sup>1,a</sup> Kai Xie,<sup>1,a,b</sup> Yanming Liu,<sup>1</sup> and Yuanyuan Yu<sup>1</sup>  
<sup>1</sup>*School of Aerospace Science and Technology, Xidian University, Xi'an 710126, China*

(Received 4 August 2017; accepted 10 October 2017; published online 19 October 2017)

A hypersonic flight or a reentry vehicle is surrounded by a plasma layer that prevents electromagnetic wave transmission, which results in radio blackout. The magnetic-window method is considered a promising means to mitigate reentry communication blackout. However, the real application of this method is limited because of the need for strong magnetic fields. To reduce the required magnetic field strength, a novel method that applies a traveling magnetic field (TMF) is proposed in this study. A mathematical model based on magneto-hydrodynamic theory is adopted to analyze the effect of TMF on plasma. The mitigating effects of the TMF on the blackout of typical frequency bands, including L-, S-, and C-bands, are demonstrated. Results indicate that a significant reduction of plasma density occurs in the magnetic-window region by applying a TMF, and the reduction ratio is positively correlated with the velocity of the TMF. The required traveling velocities for eliminating the blackout of the Global Positioning System (GPS) and the typical telemetry system are also discussed. Compared with the constant magnetic-window method, the TMF method needs lower magnetic field strength and is easier to realize in the engineering field. © 2017 Author(s). All article content, except where otherwise noted, is licensed under a Creative Commons Attribution (CC BY) license (<http://creativecommons.org/licenses/by/4.0/>). <https://doi.org/10.1063/1.4999039>

### I. INTRODUCTION

Hypersonic flight and spacecraft reentry are associated with the appearance of shock waves in front of the vehicle, converting much of the vehicle's kinetic energy into heat and increasing the air temperature. Thus, the air molecules are dissociated and ionized. Moreover, a plasma layer is created around the leading edge of the vehicle owing to the ionization of neutral particles by shock wave heating, which prevents radio communication,<sup>1</sup> a phenomenon commonly called "radio blackout." The blackout problem affects the capture and tracking ability of ground stations, as well as the transmission efficiency of real-time telemetry data and navigation information, resulting in unpredictable consequences and even disasters for some aerospace missions.

During the last 50 years, several approaches have been proposed to alleviate the radio blackout problems associated with the reentry plasma sheath,<sup>1-8</sup> such as aerodynamic shaping, electrophilic injection, high radio frequencies, high transmission power, Raman scattering, and magnetic window. However, some approaches create some disadvantages that subsequently become obstacles. For instance, to reduce sheath thickness, the reentry vehicle must be as sharply pointed as possible, which reduces the payload capacity and increases the aerodynamic heating of the vehicle.<sup>2</sup> High transmission power creates an electrical breakdown of the atmosphere, further ionizing the air and contributing to the original problem.<sup>3</sup> Therefore, we should develop a reliable and effective mitigation scheme for communication through the plasma layer. Although the magnetic window has some limitations, it is considered the most promising method for blackout mitigation.<sup>9-15</sup>

<sup>a</sup>These authors contributed equally

<sup>b</sup>Corresponding author: [kaixie@mail.xidian.edu.cn](mailto:kaixie@mail.xidian.edu.cn)

Hodara first proposed the magnetic field mitigation techniques in the 1960s and found that the magnetic field lines must be oriented such that the electrons are tightly bound to them through gyration and do not respond to the electric field component of the electromagnetic (EM) wave.<sup>9</sup> An experimental test to measure the effects of a magnetic field on Very High Frequency (VHF) waves propagation in plasma layer was carried out in the 1960s,<sup>10</sup> and the results indicated that the signal attenuation is reduced from 45 dB for zero-field to 28 dB at a 0.75 T magnetic field. Rawhouser indicated that 1.3 T is required for an S-band frequency EM wave.<sup>11</sup> Several theoretical studies on the magnetic-window method have been performed, where evidence showed that reentry blackout can be mitigated by the magnetic-field approach.<sup>12–15</sup> The interaction of the electromagnetic wave with the plasma layer is modeled using multi-fluid equations for fluid transport and full Maxwell's equations for the electromagnetic fields.<sup>12</sup> Numerical results verified that a whistler wave can propagate in plasma slab with low attenuation and has a cutoff at the electron cyclotron frequency. However, the required strong magnetic field is an obstacle in implementing the magnetic-window method. The stronger magnetic field need a heavier magnet which may result in the vehicle overload.

Considerable effort has been exerted toward addressing the problem associated with decreasing the required magnetic field.<sup>16–21</sup> An electromagnetic E×B layer approach was proposed for this problem and analyzed by a magneto-hydrodynamic model.<sup>16</sup> Simulation results showed that the application crosses electric and magnetic fields, reduces the plasma density near the antenna, and enables radio communication across the plasma. Cheng<sup>21</sup> discussed the effect of electron collisions on the required applied electromagnetic field and gave the feasible regions of the applied electromagnetic fields for eliminating blackout. However, in an E×B configuration,<sup>22</sup> the electrode was exposed in the plasma and the erosion of electrode by the high-temperature gas could a potential issue in the E×B mitigation scheme. A new method to mitigate radio blackout by using a traveling magnetic field (TMF) is presented in this paper. The TMF is used to control the liquid metal flow by Lorentz force<sup>23–25</sup> and the flow velocity of liquid metal associated with the TMF velocity. Thus, when the TMF is applied, the electrons and ions will be bound to the magnetic field and will move with the magnetic field. Plasma density will be reduced and a window will be created in a plasma layer through which EM waves can be transmitted. Theory analysis can help to estimate the effect and determine the optimal TMF configuration. For this purpose, the effect of TMF on reentry blackout mitigation is investigated in this paper.

This paper is organized as follows. First, the mitigation scheme configuration through TMF is described in Section II. A mathematical model to describe the effectiveness of this scheme based on the magneto-hydrodynamics (MHD) approach is also proposed in Section II. The EM wave propagation in TMF region is introduced in Section III. Simulation results and discussion are presented in Section IV, followed by a conclusion in Section V.

## II. THEORETICAL ANALYSIS OF TMF APPROACH FOR MITIGATING BLACKOUT

TMF, which is widely used in metallurgy and cast, is generated by a TMF electromagnetic inductor.<sup>26</sup> An air-gap magnetic field is generated by applying the three-phase symmetrical current on the three-phase winding of a linear motor. Ref. 27 shows the ideal magnetic field line of TMF is a sinusoid and can be expressed as follows:

$$\mathbf{B} = B_0 \cos(\omega_s t - k_T x) \hat{\mathbf{z}}, \quad (1)$$

where  $B_0$  is the amplitude of TMF,  $\omega_s$  is the angular frequency of the three-phase current, and  $k_T$  is the wave number of TMF. The traveling velocity of TMF can then be described as follows:

$$v_b = \frac{\omega_s}{k_T} \quad (2)$$

The schematic configuration of the TMF approach is shown in Fig. 1. An embedded electromagnet integrated beneath the antenna window will create the TMF. Through applying a certain excitation on the electromagnet, the magnetic line, which can confine the charge particles, will expand opposite the direction of plasma flow, and the plasma density will be reduced significantly. The detailed theoretical analysis of TMF approach is introduced in this section.

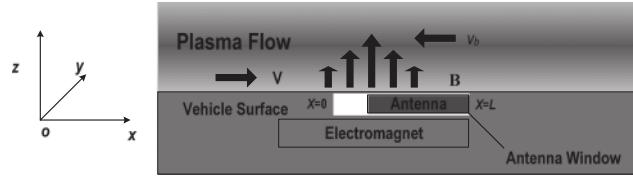


FIG. 1. Schematic of the TMF method.

A steady-state fluid plasma model<sup>16</sup> for plasma layer based on the basic equations of MHD is used to discuss the effects of TMF on a plasma flow field. The following general assumptions are made:<sup>18</sup>

- 1) The plasma near the TMF electromagnetic inductor is quasi-neutral.
- 2) Ionization in the plasma layer is not considered.
- 3) The electron temperature  $T_e$  is constant.
- 4) The magnetic field is one-dimensional ( $z$  direction) and uniform in the  $z$  direction.

The following system of equations can describe the effect of TMF. Faradays law is given by the following equation:

$$\nabla \times \mathbf{E} = -\frac{\partial \mathbf{B}}{\partial t}, \quad (3)$$

where,  $\mathbf{E}$  is the induced electric field. The mass conservation equation for the charged particles is written as follows:

$$\nabla \cdot (n_\alpha \mathbf{V}_\alpha) = 0 \quad (4)$$

The momentum conservation equation is

$$m_\alpha n_\alpha (\mathbf{V}_\alpha \cdot \nabla \mathbf{V}_\alpha) = q_\alpha n_\alpha (\mathbf{E} + \mathbf{V}_\alpha \times \mathbf{B}) - \nabla p_\alpha - \sum_{\substack{\beta=i,e,n \\ \beta \neq \alpha}} m_\alpha n_\alpha \nu_{\alpha\beta} (\mathbf{V}_\alpha - \mathbf{V}_\beta) \quad (5)$$

The equation of state of ideal gas is

$$p_\alpha = n_\alpha k_B T_\alpha, \quad (6)$$

where  $q$ ,  $n$ ,  $\mathbf{V}$ ,  $p$ ,  $T$ , and  $m$  are the charge, density, velocity vector, thermal press, temperature, and mass of charged particles, respectively. The subscript  $\alpha$  represents the types of particle fluid, where  $\alpha = i, e$ , and  $n$  denote ion fluid, electron fluid, and neutral fluid, respectively.  $\nu_{ie}$  is the ion–electron collision frequency,  $\nu_{in}$  is the ion–neutral collision frequency, and  $\nu_{en}$  is the electron–neutral collision frequency.  $k_B$  is the Boltzmann constant.

The  $\nu_{ie}$  is small enough to be neglected in comparison with the  $\nu_{en}$  and  $\nu_{in}$ . Given that the ion has a mass  $10^4$  to  $10^5$  times greater than the electron and the inertia term of the electron is small enough to be neglected, then  $m_e n_e (\mathbf{V}_e \cdot \nabla \mathbf{V}_e)$  can be approximately zeros in Equation (5).<sup>28,29</sup> The velocity  $\mathbf{V}_n$  of neutral particles approximately equals the flow velocity  $\mathbf{V}$  of the plasma layer.<sup>21</sup> With neglecting electron momentum inertia term and ion–electron collisions, Equation (5) for ion and electron can be simplified as

$$m_i n_i (\mathbf{V}_i \cdot \nabla \mathbf{V}_i) = e n_i (\mathbf{E} + \mathbf{V}_i \times \mathbf{B}) - k_B T_i \nabla n_i - m_i n_i \nu_{en} (\mathbf{V}_i - \mathbf{V}) \quad (7)$$

and

$$0 = -e n_e (\mathbf{E} + \mathbf{V}_e \times \mathbf{B}) - k_B T_e \nabla n_e - m_e n_e \nu_{en} (\mathbf{V}_e - \mathbf{V}). \quad (8)$$

To simplify the system of equations, the plasma velocity can be defined as follows:<sup>18</sup>

$$\mathbf{V} = \frac{m_i \mathbf{V}_i + m_e \mathbf{V}_e}{m_i + m_e}. \quad (9)$$

As the ion mass is much heavier than the electron mass, the plasma velocity is approximately the same as the velocity of the ions,  $\mathbf{V} \approx \mathbf{V}_i$ . By using the quasi-neutral assumption, we can express the relation between ion density and electron density as<sup>21</sup>

$$n_i \approx n_e \approx n. \quad (10)$$

Thus, Equation (4) can be transformed into

$$\nabla \cdot (n\mathbf{V}) = 0. \quad (11)$$

Equations (7) and (8) become

$$m_i n (\mathbf{V} \cdot \nabla \mathbf{V}) = en(\mathbf{E} + \mathbf{V} \times \mathbf{B}) - k_B T_i \nabla n \quad (12)$$

and

$$0 = -en(\mathbf{E} + \mathbf{V}_e \times \mathbf{B}) - k_B T_e \nabla n + m_e n v_{en} (\mathbf{V}_i - \mathbf{V}_e). \quad (13)$$

The sum of Equations (12) and (13) then provides the following momentum equation:

$$m_i n (\mathbf{V} \cdot \nabla \mathbf{V}) = en(\mathbf{V}_i - \mathbf{V}_e) \times \mathbf{B} - k_B (T_i + T_e) \nabla n + m_e n v_{en} (\mathbf{V}_i - \mathbf{V}_e), \quad (14)$$

where  $v_{en} = 6.3 \times 10^{-3} n_n (T/300)^{-1/2}$ ,<sup>30</sup>  $n_n$  is the neutral density,  $T$  is the gas temperature.

The scalar equation of Equation (14) in the x axis direction is as follows:

$$m_i n V_x \cdot \frac{dV_x}{dx} = en V_{iy} B_z - en V_{ey} B_z - k_B (T_i + T_e) \frac{dn}{dx} + m_e n v_{en} (V_{ix} - V_{ex}). \quad (15)$$

$V_{ey}$  and  $V_{iy}$  are the electron drift velocity and ion drift velocity, respectively, caused by Lorenz force.  $B_z$  is the z direction component of  $\mathbf{B}$ . From ref. 31, the electron drift velocity can be expressed as

$$V_{ey} = \gamma V_{ex} = \frac{\omega_e}{v_{en}} V_{ex}, \quad (16)$$

where  $\omega_e$  is the electron cyclotron frequency, and  $\gamma$  is the Hall parameter. Then, by submitting Equation (16) into Equation (15), we have

$$m_i n V_x \cdot \frac{dV_x}{dx} = -k_B (T_i + T_e) \frac{dn}{dx} + en V_{iy} B_z - \gamma_e en B_z V_{ix} + (\gamma_e en B_z + m_e n v_{en}) (V_{ix} - V_{ex}). \quad (17)$$

Typically, the axial velocity  $V_{ix}$  is much larger than  $V_{iy}$ . Thus,  $V_{iy}$  can be ignored, and via Equation (9), we obtain  $V \approx V_i \approx V_{ix} \approx V_x$ . In addition, the current density in the particle drift direction is small enough to be negligible in comparison with the current density in the x-direction.<sup>31</sup> Therefore, the current generation due to the particle drift is assumed to be zero. Thus, Equation (17) can be rewritten as

$$\frac{dV}{dx} = \frac{-k_B (T_i + T_e) dn}{m_i n V dx} - \frac{\gamma_e e B_z}{m_i} + \left( \frac{\gamma_e B_z}{m_i n V} + \frac{m_e v_{en}}{m_i n V e} \right) J, \quad (18)$$

where the definition of the current density,  $J = en (V_{ix} - V_{ex})$ , is used to simplify the equation.

For the one-dimensional case,  $nV$  is a constant from Equation (11):

$$n_0 V_0 = nV, \quad (19)$$

where  $n_0$  and  $V_0$  are the initial plasma density and plasma velocity at the edge of antenna window  $x = 0$ , respectively. From Equation (11), we also obtain

$$\frac{dn}{dx} = -\frac{n}{V} \frac{dV}{dx}. \quad (20)$$

By submitting Equations (1), (19), and (20) into Equation (18), the differential equation for plasma velocity can be obtained as

$$\left(1 - \frac{k_B (T_i + T_e)}{m_i V^2}\right) dV = \left[ \frac{\gamma_e B_0 \cos(\omega t - kx)}{m_i} \left(\frac{j}{n_0 V_0} - e\right) + \frac{m_e v_{en}}{m_i n_0 V_0 e} J \right] dx. \quad (21)$$

The current density conservation in plasma is given in ref. 18:

$$\nabla \cdot \mathbf{J} = 0. \quad (22)$$

For the one-dimensional case, Equation (22) makes using a constant current density assumption possible. Thus, Equation (21) can be solved as follows:

$$\left[ V + \frac{k_B(T_i + T_e)}{m_i V} \right] - \left[ V_0 + \frac{k_B(T_i + T_e)}{m_i V_0} \right] = \frac{\gamma_e}{m_i k} \left( e - \frac{J}{n_0 V_0} \right) B_0 \sin(\omega_s t - k_T x) + \frac{m_e \nu_{en} J}{m_i n_0 V_0 e} x. \quad (23)$$

By solving Equation (23) and using Equations (2) and (19), we can derive the reduction ratio which presents the ratio of the plasma density with TMF to initial plasma density  $N(x) = n(x)/n_0$  as

$$N(x) = \frac{2V_0}{\left[ a + \frac{bv_b}{\omega_s} B_0 \sin(\omega(t - v_b x)) + cx \right] + \sqrt{\left[ a + \frac{bv_b}{\omega_s} B_0 \sin(\omega(t - v_b x)) + cx \right]^2 - 4d}}, \quad (24)$$

$$\text{where } a = \left[ V_0 + \frac{k_B(T_i + T_e)}{m_i V_0} \right], b = \frac{\gamma_e}{m_i} \left( e - \frac{j}{n_0 V_0} \right), c = \frac{m_e \nu_{en} j x}{m_i n_0 V_0 e}, d = \frac{k_B(T_i + T_e)}{m_i}.$$

Known from the definition of the reduction ratio  $N$ , a lower reduction ratio means a stronger plasma density reduction. From Equation (24), the plasma density reduces with increasing magnetic field strength or traveling velocity. As such, when using a TMF approach to mitigate blackout, traveling velocity, instead of magnetic field, can be increased to avoid the addition of weight to the system. Details about the simulations and discussions are presented in Section IV.

### III. PROPAGATION PROPERTIES OF EM WAVE IN TMF REGION

With the above expression for the electron density reduction, the next step is to relate the propagation properties of EM wave in the TMF region. The transmission coefficient of EM wave is a crucial parameter in describing EM waves propagating through dielectric media, on which the criteria for reentry blackout are based. Therefore, we present an analysis of the transmission coefficient in the TMF region.

As indicated in refs. 3 and 32–34, the antennas are located at the after body of vehicle, where the plasma has lower electron density and are more stable. Thus, the fluctuation of plasma density is not considered in this paper. The electron density plasma layer is consider as uniform. In addition, in this study, the applied magnetic field is less than 0.15 T, which is the maximum magnetic field under the existing technical level; the magnetization of the plasma can be ignored because the relative errors between the results with and without considering magnetization are less than 8%.<sup>21</sup> On the basis of the above expression, the complex permittivity of the plasma layer can be determined as

$$\varepsilon = \left( 1 - \frac{\omega_p^2}{\omega^2 + \nu_{en}^2} - j \frac{\omega_p^2 \nu_{en} / \omega}{\omega^2 + \nu_{en}^2} \right) \varepsilon_0, \quad (25)$$

where  $\varepsilon_0$  is the permittivity of vacuum,  $\omega$  is the angular frequency of EM wave, and  $\omega_p$  is the plasma resonant frequency and is described as  $\omega_p = \sqrt{n_e e^2 / \varepsilon_0 m_e}$ . The EM characteristics of the plasma layer can be established by combining the plasma frequency  $\omega_p$  and the collision frequency  $\nu$  of plasma layer.

Fig. 2 illustrates the geometric sketch of EM waves propagating in a plasma player model in consideration of EM waves propagating in the  $xoz$  plane. The layer 1 and layer 3 are air. For the  $n$ th layer,  $E_{ni}$  and  $H_{ni}$  represent the electric and magnetic fields of incident wave, respectively, and  $E_{nr}$  and  $H_{nr}$  are the fields of reflect wave. The electric field and magnetic field in layer 1 can be described as

$$\begin{aligned} E_1 &= \mathbf{e}_x \left[ E_{1i} e^{-jk_1 z} + E_{1r} e^{jk_1 z} \right] \\ H_1 &= \mathbf{e}_y \frac{1}{\eta_1} \left[ E_{1i} e^{-jk_1 z} - E_{1r} e^{jk_1 z} \right], \end{aligned} \quad (26)$$

the fields in plasma layer are

$$\begin{aligned} E_{2i} &= \mathbf{e}_x \left[ E_{2i} e^{-jk_2(z-d)} + E_{2r} e^{jk_2(z-d)} \right] \\ H_{2i} &= \mathbf{e}_x \frac{1}{\eta_2} \left[ \left[ E_{2i} e^{-jk_2(z-d)} - E_{2r} e^{jk_2(z-d)} \right] \right], \end{aligned} \quad (27)$$

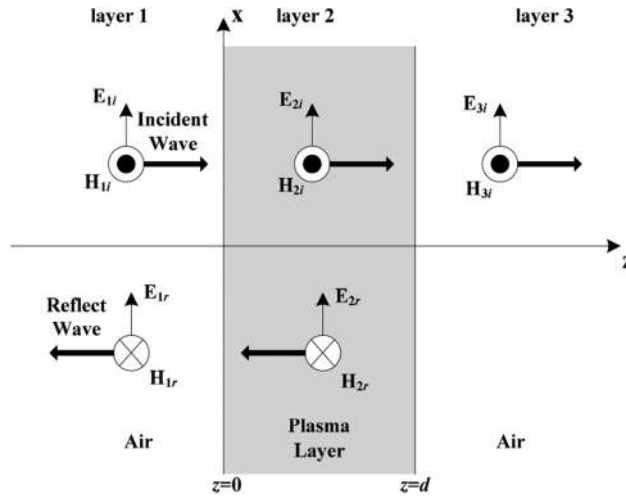


FIG. 2. Geometry of EM wave propagation in the plasma layer.

and the fields in layer  $n+1$  are

$$E_3 = \mathbf{e}_x E_{3i} e^{-jk_3(z-d)}$$

$$H_3 = \mathbf{e}_y \frac{1}{\eta_{n+1}} E_{3i} e^{-jk_3(z-d)}$$
(28)

Here,  $k_n = \omega \sqrt{\mu_0 \epsilon_n}$  is the EM wave vector,  $\eta_n = \sqrt{\mu_0 / \epsilon_n}$  denotes the EM wave impedance, and  $d$  is the thickness of the plasma layer. By the continuous boundary condition of two adjacent layers, the transmission coefficient  $\Lambda$  and reflection coefficient  $\Gamma$  between layer 2 and layer 3 can be yielded as follows:

$$\Gamma_2 = \frac{\eta_3 - \eta_2}{\eta_3 + \eta_2}$$

$$\Lambda_2 = 1 + \Gamma_2$$
(29)

The parameters between layer 1 and layer 2 can be written as

$$Z = \eta_2 \frac{1 + \Gamma_2 e^{-j2k_2 d}}{1 - \Gamma_2 e^{-j2k_2 d}}$$

$$\Gamma_1 = \frac{Z - \eta_1}{Z + \eta_1}$$

$$\Lambda_1 = \frac{(1 + \Gamma_1) e^{-jk_2 d}}{1 + \Gamma_2 e^{-j2k_2 d}}$$
(30)

where  $Z$  is the equivalent wave impedance for plasma layer. Then, the total transmission coefficient is obtained as follows:

$$\Lambda = \Lambda_1 \cdot \Lambda_2$$
(31)

#### IV. SIMULATION RESULTS AND DISCUSSION

According to typical data collected in the RAM-C project conducted by NASA,<sup>35</sup> significant signal attenuation occurs when the reentry altitudes are between 30 and 70 km, where the peak electron densities near the antenna window are approximately  $10^{17}$ – $10^{19}/\text{m}^3$ . Thus, we pay more attention to this region and present the simulation results of the TMF approach efficiency for mitigating blackout in this section. The other parameters are listed as follows: plasma layer thickness is 0.05 m, collision frequency is set to 1 GHz according to ref. 3, and flow velocity<sup>36</sup> is  $V_0 = \sqrt{k_B T_e / m_e}$ . The range of electron temperature during reentry is 2–6 eV.<sup>36</sup> The current density  $J$  is a constant and taken as  $200 \text{ A/m}^2$ .<sup>21</sup> The width of antenna window  $L$  is set to 0.15 m because the antenna sizes are

considered. The frequency of the three-phase current  $f_s$  is 500 Hz. We consider the case that  $\omega_s t$  is equal to  $k_T L + \pi/2$  when a maximum magnetic field appears and  $B_0 = 0.15$  T is limited by system weight.

### A. Effect of TMF on electron density

This part investigates the effects of TMF on plasma with different electron densities and TMF velocities. From Equation (24), the reduction ratio  $N$  varies with traveling velocity  $v_b$  and initial velocity of plasma flow  $V_0$ , which is a function of electron temperature  $T_e$ . The reductions ratio versus initial plasma density with traveling velocity or initial velocity of plasma flow as a parameter are shown in Fig. 3. In the figure, the TMF approach leads to a strong plasma density reduction. It also shows that when the initial plasma density is lower than  $10^{18}/\text{m}^3$ , the reduction ratio  $N$  decreases rapidly with the increased  $n_0$  and  $N$  flattens out with  $n_0$  continuing to increase. Large plasma density has great conductivity and leads to large inductive current and strong Lorentz force caused by TMF. Thus, plasma density reduction becomes stronger. As shown in Fig. 3(a), the reduction ratio  $N$  decreases with increased  $v_b$ . For instance, in the case of  $n_0 = 10^{18}/\text{m}^3$ , when the  $v_b$  varies from 30 m/s to 100 m/s, the reduction ratio  $N$  changes from 0.34 to 0.15. The electron temperature also affects the reduction ratio, as shown in Fig. 3(b), but this is weaker than that of the traveling velocity. It follows from Fig. 3(b) that a higher electron temperature lead to larger the reduction ratio  $N$  which means the weaker plasma density reduction. A larger electron temperature means a larger initial velocity; the larger the plasma initial velocity, the more difficult it is to change the plasma density.<sup>16</sup>

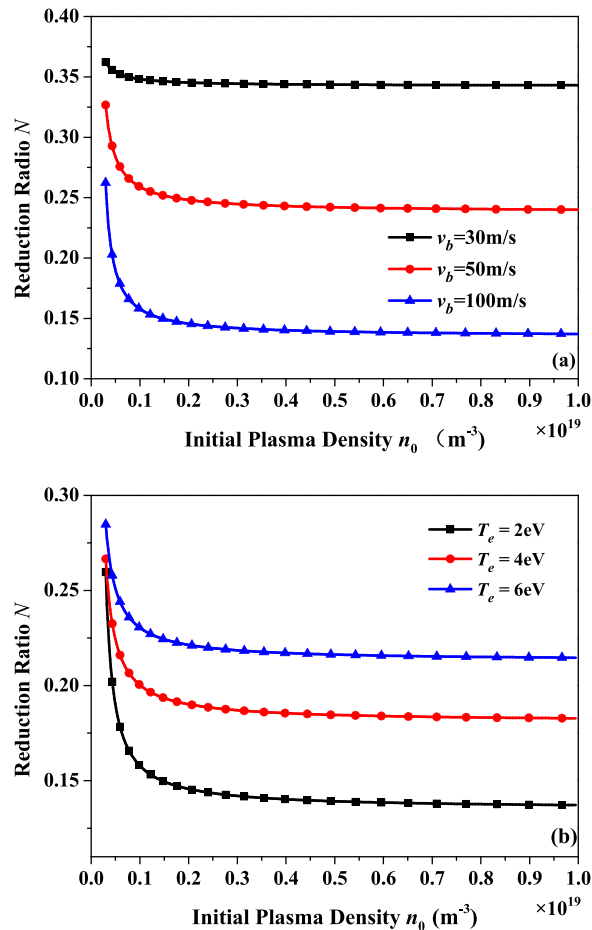


FIG. 3. Reduction ratio versus initial plasma density with (a) traveling velocity as a parameter;  $T_e = 2$  eV, and (b) electron temperature as a parameter;  $v_b = 100$  m/s.



However, in a real system, the electron temperature (plasma initial velocity) is difficult to control. Thus, by limiting the magnetic field strength, the effectiveness of the TMF approach for blackout mitigation can only be improved by traveling velocity.

To analyze the effect of traveling velocity on plasma density reduction in detail, the reduction ratio under TMF at different field velocities is plotted in Fig. 4. A most significant plasma density reduction can be achieved by increasing the traveling velocity. In Fig. 4(a), a higher initial plasma density gets a stronger plasma density reduction with the increased traveling velocity. For instance, when the initial plasma density is low, such as  $n_0=1\times 10^{17}/\text{m}^3$ , the reduction ratio  $N$  is decreased from 0.33 to 0.086, with the traveling velocity increasing from 10 m/s to 1000 m/s and the relative reduction ratio  $r_n = 17.74$  ( $r_n = N_{max}/N_{min}$ , which presents the ratio of the maximum plasma density to the minimum plasma density under the same  $n_0$  and range of  $v_b$ ). By contrast, for  $n_0=5\times 10^{18}/\text{m}^3$ , the plasma density  $N$  decreases from 0.59 to 0.016, where the  $r_n = 36.86$  under the same condition. The curves of  $n_0=5\times 10^{18}/\text{m}^3$  and  $n_0=1\times 10^{19}/\text{m}^3$  overlap; that is,  $r_n$  has a limitation for different  $n_0$  and the same range of  $v_b$ . Meanwhile, with the traveling velocity increasing, the plasma density can be reduced by approximately two orders of magnitude, which may be sufficient to allow radio communication.

As show in Fig. 4(a), the reduction ratio curves become flat, when the traveling velocity is larger. For instance, when  $n_0=1\times 10^{19}/\text{m}^3$ , the reduction ratio decrease from 0.6 to 0.03 with the traveling velocity increasing from 10m/s to 500m/s, and the reduction ratio decrease from 0.03 to 0.015 with the traveling velocity increasing from 500m/s to 1000m/s. It means that the reduction ratio decrease slowly, when the traveling velocity is larger. Thus, the relative reduction ratio  $\Delta N$

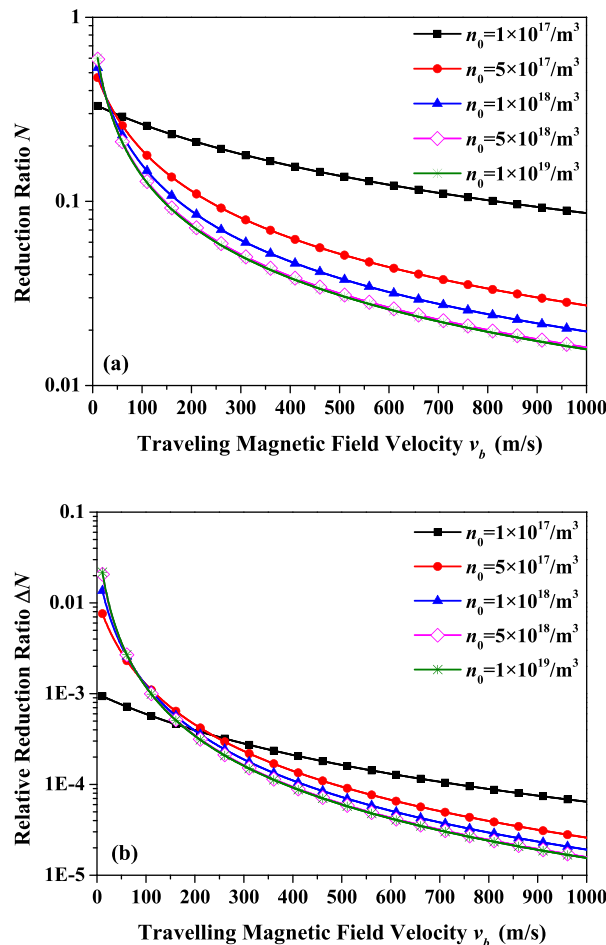


FIG. 4. Reduction ratio versus traveling velocity;  $T_e = 2\text{eV}$  (a) reduction ratio (b) relative reduction ratio.

defined to analyze the efficiency of plasma density reduction during the increase of traveling velocity. Here,  $\Delta N = |N_{v_b+\Delta v} - N_{v_b}|$ , where  $N_{v_b}$  is the reduction ratio  $N$  corresponding to the traveling velocity  $v_b$ . The relative reduction ratio  $\Delta N$  is the absolute variation of reduction ratio  $N$ , when the traveling velocity adds  $\Delta v$ , and represents efficiency of plasma density reduction during the increase of traveling velocity. The smaller the relative reduction ratio  $\Delta N$ , the lower the efficiency. In this section,  $\Delta v$  is set to 1m/s and the relative reduction ratio  $\Delta N$  is plotted in Fig. 4(b). As shown in Fig. 4(b),  $\Delta N$  decreases with increasing  $v_b$ . For instance, when  $n_0=1\times 10^{19}/\text{m}^3$ , the relative reduction ratios can reach  $10^{-3}$  for  $v_b = 100$  m/s, and  $10^{-4}$  for  $v_b = 500$  m/s. It means that the higher the traveling velocity, the lower efficiency. Thus, the efficiency of increasing velocity must be considered when the velocity of the applied magnetic field is optimized.

## B. Blackout mitigation effectiveness of typical frequency EM wave

With respect to NASA test data, blackout occurs when the attenuation of EM wave exceeds 30 dB.<sup>3,37</sup> High-frequency waves can pass through plasma with low attenuation. However, several communication systems cannot change their working frequency band, such as L band (1.575 GHz) for GPS, S band (2.3 GHz) for telemetry, and C band (5.7 GHz) for communication with satellite. Thus, the TMF approach can mitigate radio blackout when a low-frequency communication system is used. To optimize the velocity of applied magnetic field for different typical frequency waves, the transmission coefficients of L, S, and C band EM wave propagation in plasma versus different  $v_b$  are shown in Fig. 5. The plasma densities  $n_e$  in equation are taken as  $1\times 10^{18}/\text{m}^3$ ,  $5\times 10^{18}/\text{m}^3$ , and  $1\times 10^{19}/\text{m}^3$  for most of the severe blackout reentry altitudes.<sup>35</sup> The electron temperature set as 2eV.

Fig. 5 shows the shadow area where the attenuation exceeds 30 dB can be regarded as a blackout region. The dash line is the original attenuation without magnetic field, and the full curve represents the wave attenuation under TMF. Fig. 5 shows all three electron densities can lead to radio blackout for the L, S, and C band waves without using magnetic field. Attenuation of the EM wave can be reduced by applying TMF, and the blackout caused by a lower plasma density requires a lower traveling velocity for mitigation. In Fig. 5(a), for the L band wave, when the TMF is applied, the GPS signal can pass through plasma when  $v_b > 62$  m/s for  $n_e = 1\times 10^{18}/\text{m}^3$ ,  $v_b > 345$  m/s for  $n_e = 5\times 10^{18}/\text{m}^3$  and  $v_b > 690$  m/s for  $n_e = 1\times 10^{19}/\text{m}^3$ . Similarly, the effect of TMF on the C band wave can be seen from Fig. 5(b): the minimum required velocities are 50, 290, and 605 m/s for  $n_e = 1\times 10^{18}/\text{m}^3$ ,  $5\times 10^{18}/\text{m}^3$ , and  $1\times 10^{19}/\text{m}^3$ , respectively. Compared with the results in Fig. 5(a), the required velocity decreases with the increasing wave frequency. A significant mitigation effect of TMF on the C band wave is shown in Fig. 5(c). When the  $5\times 10^{18}/\text{m}^3$ , a TMF with about 125m/s can satisfy the requirement. Even if the plasma density is  $1\times 10^{19}/\text{m}^3$ , the traveling velocity requires only about 263m/s, which is much lower than the same case for the L and S bands. In conclusion, the TMF approach can be used to mitigate radio blackout by controlling the traveling velocity instead of magnetic field strength. Meanwhile, a low velocity, which can be easily achieved, is required for all three bands when the plasma density is lower than or near  $10^{18}/\text{m}^3$ . Only C band radio blackout can be eliminated with high plasma density when the traveling velocity is low.

The characteristic of EM wave propagation in plasma under time-varying magnetic field which is the property of traveling magnetic field is discussed in following part. In this paper, the frequency of magnetic field is 500 Hz, which is much lower than the EM wave frequency. Thus, the antenna which is used for receiving high frequency EM wave cannot receive the wave generate by time-varying magnetic field. Moreover, the low frequency wave is attenuated by plasma significantly. Therefore, the effect of time-varying magnetic field on EM radiation is neglected. In simulation, the initial plasma densities set as  $5\times 10^{18}/\text{m}^3$ , the collision frequency is 1GHz, the traveling velocity is 100m/s, 200 m/s and 500 m/s, and the electron temperature is 2 eV. The transmission coefficients of L, S, and C band EM wave propagation in different plasmas versus time  $t$  are shown in Fig. 6. As shown in Fig. 6, the attenuation of EM wave varies periodically with the time  $t$ , and the period of EM wave attenuation is 1 ms which is half of the time-varying magnetic field period. For each curve contain the low attenuation region and the high attenuation region. The EM wave can pass through plasma at low attenuation region and is cut-off at high attenuation region. Thus, the wider the time range of

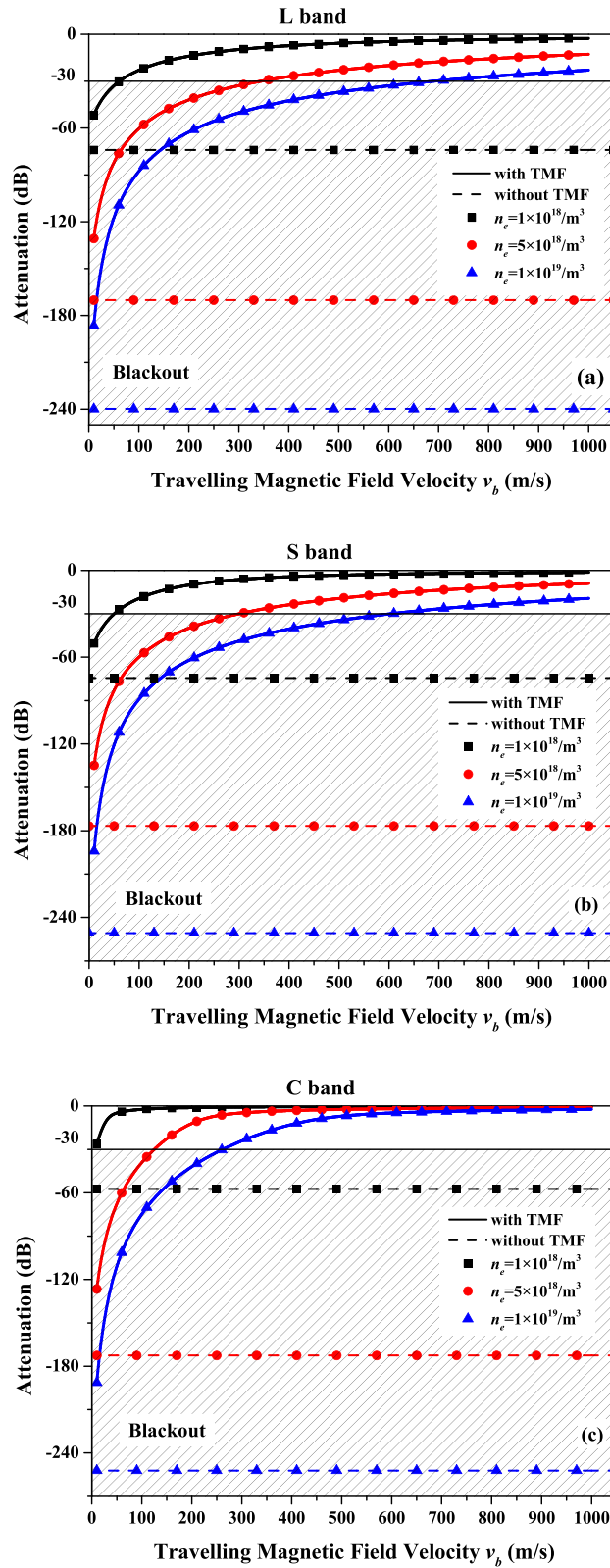


FIG. 5. Attenuation of typical frequency wave versus traveling velocity under different plasma densities;  $T_e = 2\text{eV}$  (a) L band (1.575 GHz); (b) S band (2.3 GHz); (c) C band (5.7 GHz).

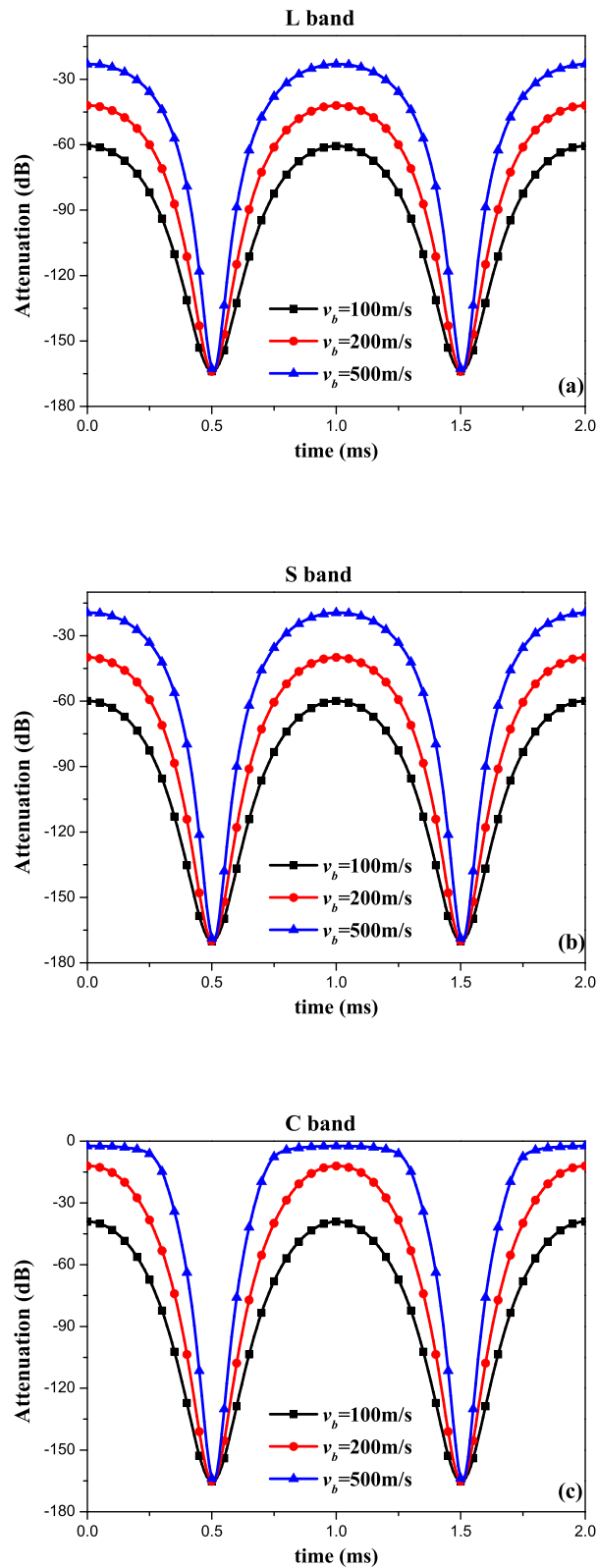


FIG. 6. Attenuation of typical frequency wave versus times under different traveling velocities;  $T_e = 2$  eV (a) L band (1.575 GHz); (b) S band (2.3 GHz); (c) C band (5.7 GHz).

low attenuation region, the better the blackout mitigation effect. It can be seen from Fig. 6, with the traveling velocity increasing, the time range of low attenuation region is increased and the actuation of EM wave in low attenuation region is reduced. For instance, the time ranges of low attenuation are about 0.4 ms, 1 ms and 1.5 ms for  $v_b=100$  m/s, 200 m/s and 500 m/s at one magnetic field period in Fig 6. (a). Similar results are shown in Figs. 6 (b) and (c) for S and C band. Moreover, comparing with Figs. 6 (a), (b) and (c), the larger frequency EM wave has a wider range of low attenuation region. Therefore, the effect of time-varying magnetic field on EM wave propagation can be reduced by increasing the TMF traveling velocity, especially for high frequency EM wave.

## V. CONCLUSION

As a promising scheme in eliminating the communication blackout, magnetic-window method requires a strong magnetic field, which is limited by technical level and system weight, to reduce the attenuation of EM wave propagation in plasma. Thus, a strong magnetic field restricts the application of the magnetic-window method in actual reentry vehicles. The TMF approach as a blackout mitigation scheme is proposed to reduce the required magnetic field. Based on the MHD theory and EM wave propagation theory, an analytical model is presented to describe the effectiveness of TMF mitigation approach in removing the reentry blackout. The simulation results show that the plasma density can be reduced significantly when a TMF is applied. Instead of increasing the magnetic field, the EM wave can be permitted to pass through the plasma sheath by adapting the traveling velocity. The required TMF velocities to eliminate L, S and C band blackout under different plasma densities are calculated. The lower plasma density or higher wave frequency requires lower velocity.

Although progress has been made and the conclusion has important significance to the blackout problem, further work should be done in the future. Only one dimension case is considered in this paper. However, the electron density is nonuniform along the direction vertical to the vehicle surface. A three dimension analysis to model the electron density reduction is necessary in further work.

## ACKNOWLEDGMENTS

This work was supported by the National Basic Research Program of China under Grant 2014CB340204 and by the National Natural Science Foundation of China under Grants 61771370.

- <sup>1</sup> J. P. Rybak and R. J. Churchill, *IEEE Trans. Aero Elec Sys.* **7**(5), 879–894 (1970).
- <sup>2</sup> P. W. Huber and T. E. Sims, *Astronautics and Aeronautics* **2**, 30 (1964).
- <sup>3</sup> R. A. Hartunian, G. E. Stewart, S. D. Ferguson *et al.*, Cause and Mitigations Radio Frequency (RF) Blackout During Re-entry of Reusable Launch Vehicles, ATR 2007(5309)-1 (2007). The Aerospace Corporation, El Segundo, USA.
- <sup>4</sup> E. D. Gillman, J. Williams, C. S. Compton, and W. E. Amatucci, *Physics of Plasmas* **22**, 043706 (2015).
- <sup>5</sup> I. F. Belov, V. Ya. Borovoy, V. A. Gorelov *et al.*, *Journal of Spacecraft and Rockets* **38**(2), 249–256 (2001).
- <sup>6</sup> S. V. Nazarenko, A. C. Newell, and V. E. Zakharov, *Physics of Plasmas* **1**(9), 2827 (1994).
- <sup>7</sup> V. I. Sotnikov, S. Mudaliar, T. C. Genoni *et al.*, *Physics of Plasmas* **18**, 062104 (2011).
- <sup>8</sup> K. Xie, M. Yang, B. W. Bai, X. P. Li, H. Zhou, and L. X. Guo, *J. Appl. Phys.* **119**, 023301 (2016).
- <sup>9</sup> H. Hodara, *Proc. IRE* **49**(12), 1825–1830 (1961).
- <sup>10</sup> F. P. Russo and J. K. Hughes, *Measurements of the Effects of Static Magnetic Fields on VHF Transmission in Ionized Flow Fields*, TM X-907 (1964). NASA, Washington, DC, USA.
- <sup>11</sup> R. Rawhouser, “Overview of the AF Avionics Laboratory re-entry electromagnetics program,” NASA/SP-252: 3, NASA Langley Research Center. Hampton, 1970.
- <sup>12</sup> M. Kundrapu, J. Loverich, K. Beckwith *et al.*, *Journal of Spacecraft and Rockets* **52**(3), 813–862 (2015).
- <sup>13</sup> C. Thoma, D. V. Rose, C. L. Miller, R. E. Clark, and T. P. Hughes, *J. Appl. Phys.* **106**, 043301 (2009).
- <sup>14</sup> H. Zhou, X. P. Li, Y. M. Liu, B. W. Bai, and K. Xie, *IEEE. Trans. Plasma. Sci.* **45**(1), 15–23 (2017).
- <sup>15</sup> H. Zhou, X. P. Li, K. Xie *et al.*, *AIP Advances* **7**, 025114 (2017).
- <sup>16</sup> M. Keidar, M. Kim, and D. I. Boyd, *Journal of Spacecraft and Rockets* **45**(3), 445–453 (2008).
- <sup>17</sup> M. Kim, M. Keidar, and D. I. Boyd, *Journal of Spacecraft and Rockets* **45**(6), 1223–1229 (2008).
- <sup>18</sup> M. Kim, Electromagnetic manipulation of plasma layer for re-entry blackout mitigation,” [PhD] (University of Michigan, 2009).
- <sup>19</sup> M. Kim, D. I. Boyd, and M. Keidar, *Journal of Spacecraft and Rockets* **47**(1), 29–35 (2010).
- <sup>20</sup> R. L. Stenzel and J. M. Urrutia, *Journal of Applied Physics* **113**, 103303 (2013).
- <sup>21</sup> J. J. Cheng, K. Jin, and Y. Kou, *Journal of Applied Physics* **121**, 093301 (2017).
- <sup>22</sup> K. M. Lemmer, A. D. Gallimore, T. B. Smith, Davis *et al.*, *Journal of Spacecraft & Rockets* **46**(6), 1100–1109 (2009).
- <sup>23</sup> K. Ueno, *Physics of Fluids A* **3**(12), 3107–3116 (1991).
- <sup>24</sup> K. Ueno, *Physics of Fluids A* **5**(2), 490–492 (1993).
- <sup>25</sup> A. A. Tzavaras and H. D. Brody, *Journal of Metals* **36**(3), 31–37 (1984).

- <sup>26</sup> S. Yamamura, *Theory of Linear Induction Motors* (John Wiley & Sons, 1972), New York.
- <sup>27</sup> Y. S. Zhou and Y. J. Zhou, *Journal of Xuchang Teachers College* **20**(5), 11–14 (2001).
- <sup>28</sup> R. L. Merlino and N. D'Angelo, *Physics of Plasmas* **12**, 054504 (2005).
- <sup>29</sup> M. Keidar and I. I. Beilis, *IEEE Transactions on Plasma Science* **34**(3), 804–814 (2006).
- <sup>30</sup> V. L. Ginzburg, *The Propagation of Electromagnetic Waves in Plasmas* (Oxford, 1970).
- <sup>31</sup> M. Keidar, D. I. Boyd, and I. I. Beilis, *Physics of Plasmas* **8**(12), 5315–5322 (2001).
- <sup>32</sup> Z. W. Liu, W. M. Bao, X. P. Li *et al.*, *Plasma Science and Technology* **18**(2), 131–137 (2016).
- <sup>33</sup> Z. W. Liu, W. M. Bao, X. P. Li *et al.*, *Plasma Science and Technology* **18**(6), 617–626 (2016).
- <sup>34</sup> B. Bai, X. P. Li, Y. M. Liu, J. Xu, L. Shi, and K. Xie, *IEEE Trans. Plasma. Sci.* **42**(10), 3365–3371 (2014).
- <sup>35</sup> C. T. Swift, F. B. Beck, J. Thomson *et al.*, “RAM CIII S-band diagnostic experiment,” NASA-SP-252: 137 (1970), NASA Langley Research Center, Hampton.
- <sup>36</sup> K. M. Lemmer, “Use of a helicon source for development of a re-entry blackout amelioration system,” [PhD] (University of Michigan, 2009). 6.
- <sup>37</sup> K. Xie, X. P. Li, D. L. Liu, M. X. Shao, and H. L. Zhang, *Rev. Sci. Instrum* **84**, 104701 (2013).